

# Porous $\text{Co}_3\text{O}_4$ Nanotubes Derived From $\text{Co}_4(\text{CO})_{12}$ Clusters on Carbon Nanotube Templates: A Highly Efficient Material For Li-Battery Applications\*\*

By Ning Du, Hui Zhang, Bindi Chen, Jianbo Wu, Xiangyang Ma, Zhihong Liu, Yiqiang Zhang, Deren Yang,\* Xiaohua Huang, and Jiangping Tu

Over the past decades, a worldwide effort has been made to search for alternative anode materials of lithium batteries for improving their energy density and safety.<sup>[1]</sup> It has been found that 3d transition metal oxides such as nickel oxide, cobalt oxide, and iron oxide exhibit reversible capacities about three times larger than those of graphite ( $372 \text{ mAh g}^{-1}$ ) at a relative low potential, which greatly spurs the rapid development in this field.<sup>[2]</sup> Among them, cobalt oxides ( $\text{Co}_3\text{O}_4$  and  $\text{CoO}$ ) have shown the highest capacity ( $700 \text{ mAh g}^{-1}$ ) and best cycle performance (93.4 % of initial capacity was retained after 100 cycles), compared with nickel oxide ( $\text{NiO}$ ) and iron oxides ( $\text{Fe}_2\text{O}_3$  and  $\text{Fe}_3\text{O}_4$ ).<sup>[3]</sup> In recent years, the nanostructured materials have attracted great interest in the application of anode or cathode materials for lithium batteries because of their high surface-to-volume ratio and short path length for  $\text{Li}^+$  transport.<sup>[4]</sup> As a result, it is believed that the  $\text{Co}_3\text{O}_4$  nano-materials can exhibit the superior Li-battery performance.

Previously, several  $\text{Co}_3\text{O}_4$  nanostructures such as nanoparticles, nanowires, and nanotubes were prepared by different methods.<sup>[5]</sup> Among them, the nanotubes have been considered one of the most promising structures for lithium batteries due to their higher surface-to-volume ratio than other one-dimensional nanostructures such as nanowires and more difficult for aggregation in comparison with nanoparticles. By far, there is little literature about the synthesis and application of  $\text{Co}_3\text{O}_4$  nanotubes for lithium batteries.<sup>[6]</sup> For example, Chen et al. synthesized the  $\text{Co}_3\text{O}_4$  nanotubes via the anodic aluminum oxide (AAO) template route and applied them for lithium batteries with the capacity of about  $800 \text{ mAh g}^{-1}$  at the current density of  $50 \text{ mA g}^{-1}$ . However, there are some disadvantages for the AAO template assisted approach to synthesize

metal oxide nanotubes, which restrict their application in Li-battery.<sup>[7]</sup> Firstly, the mass production of metal oxide nanotubes prepared by such an approach is impracticable, which is one of the bottlenecks for their wide applications. Secondly, it is very difficult to completely remove the nanoporous alumina template. Thirdly, the diameters of metal oxide nanotubes prepared by such an approach are usually larger than 100 nm.

Recently, carbon nanotubes (CNTs) have been considered to be an ideal template for the synthesis of metal oxide nanotubes due to the mass production, being easily removed and small diameter. For example, Liu et al. reported the synthesis of  $\text{Fe}_2\text{O}_3/\text{CNTs}$  core-shell nanostructures and polycrystalline  $\text{Fe}_2$

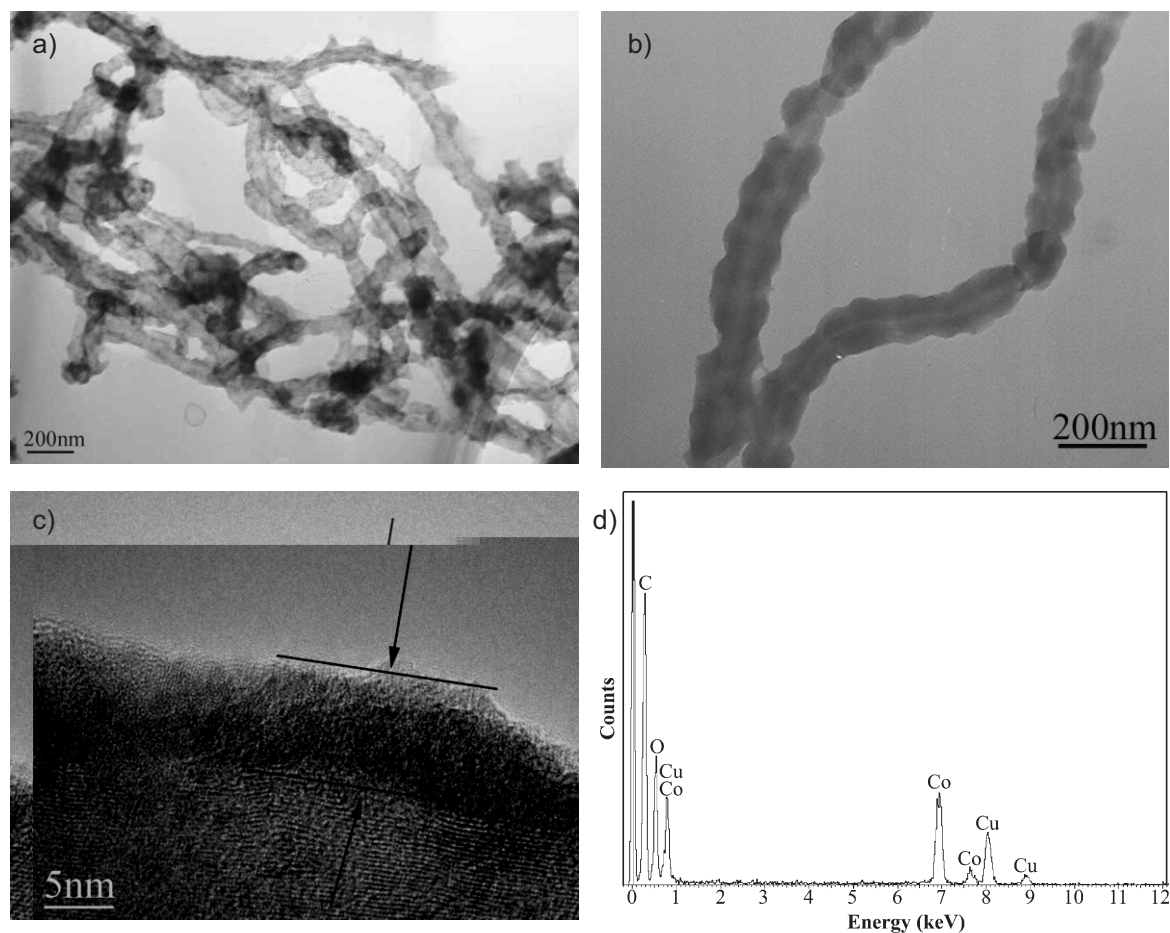
with negative charge after nitric acid treatment due to the electrostatic attraction between the charged species. With the extension of the reaction time, the shell layer of  $\text{CoO}_x$  was formed on the surface of CNTs. Finally, the porous  $\text{Co}_3\text{O}_4$  nanotubes were obtained by the calcination (the detailed growth condition can be seen in the Experimental section).



Figure 1 shows the morphological and structural characterizations of the products prepared by the sonication for 1 h at room temperature in the hexane solution of  $\text{Co}_4(\text{CO})_{12}$  and CNTs. As can be seen from the transmission electron microscopy (TEM) image (Fig. 1a), almost all CNTs have been fully coated with the thin and uniform layers. The occasional broken place marked by an arrow in Figure 1b clearly confirms the formation of CNT- $\text{CoO}_x$  nanocables. The high-resolution transmission electron microscopy (HRTEM) performed on an individual CNT- $\text{CoO}_x$  nanocable, as illustrated in Figure 1c, indicates that the thickness of the shell is usually less than

10 nm. Moreover, no observation of the lattice fringe from the part of the  $\text{CoO}_x$  shell in the HRTEM image reveals that the as-synthesized  $\text{CoO}_x$  shell is amorphous. In addition, the thickness of the  $\text{CoO}_x$  shell can be readily regulated by the ratio of CNTs to  $\text{Co}_4(\text{CO})_{12}$ . The energy dispersive X-ray (EDX) analysis of the nanocables is shown in Figure 1d. The strong peaks for Co, O and C are found in the spectrum, which corresponds to CNTs and  $\text{CoO}_x$ . While, the Cu peak comes from the Cu grid used for TEM measurements.

It has been reported that CNTs can be oxidized into  $\text{CO}_2$  above  $400^\circ\text{C}$ .<sup>[14]</sup> Therefore, after the calcination at  $500^\circ\text{C}$  in  $\text{O}_2$ , the CNTs can be completely removed and the amorphous  $\text{CoO}_x$  shell can be oxidized and crystallized. Figure 2a shows the XRD pattern of the sample after the calcination. All the diffraction peaks can be indexed as cubic  $\text{Co}_3\text{O}_4$  with the lattice constants  $a = 8.08 \text{ \AA}$ , which are consistent with the values in the standard card (JCPDS Card No.42-1467). No peaks from other phases have been detected. Moreover, the morphological characterization of the sample after the calcination is displayed in Figure 2b and c. From those images, a large quantity of the uniform  $\text{Co}_3\text{O}_4$  nanotubes with the diameter of about 30 nm can be observed. The magnified TEM image (Fig. 2d) reveals



**Figure 1.** Morphological and structural characterizations of CNTs- $\text{CoO}_x$  nanocables prepared by the sonication for 1 h at room temperature in the hexane solution of  $\text{Co}_4(\text{CO})_{12}$  and CNTs: a), b) TEM image; c) HRTEM image; d) EDX pattern.

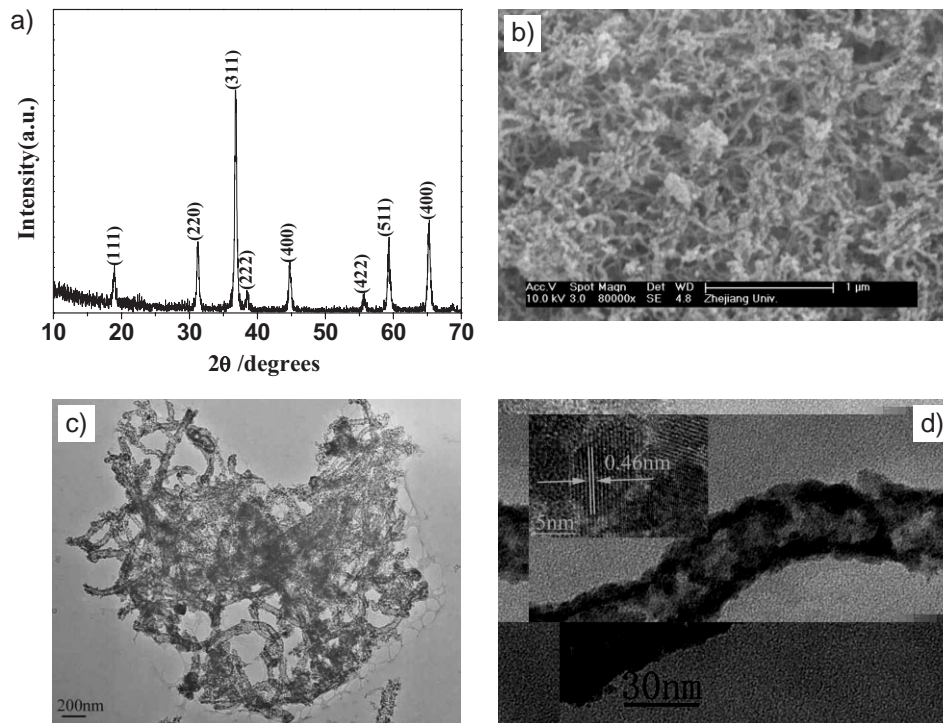


**Figure 2.** Morphological and structural characterizations of the  $\text{Co}_3\text{O}_4$  nanotubes prepared by the calcination of CNT- $\text{Co}_x$  nanocables at  $500^\circ\text{C}$  in  $\text{O}_2$  for 3 h: a) XRD pattern; b) FESEM image; c), d) TEM image. The upper-left inset in d corresponds to the HRTEM image.

that the wall thickness of the nanotubes is about 5 nm. Furthermore, there are lots of pores with the size of about several nanometers in the wall of the nanotubes due to the decomposition of CNTs, which greatly improves the surface-to-volume ratios of  $\text{Co}_3\text{O}_4$ . The inset in Figure 2d shows the HRTEM image of an individual  $\text{Co}_3\text{O}_4$  nanotube. From this image, the  $\text{Co}_3\text{O}_4$  nanotube is composed of nanoparticles with the size of about 5–10 nm, indicating that the  $\text{Co}_3\text{O}_4$  nanotubes are polycrystalline in nature. Moreover, the lattice fringes with a lattice spacing of about 0.467 nm corresponds to the {111} planes of  $\text{Co}_3\text{O}_4$ , which is consistent with the XRD results.

It has been proved that the electrochemical reaction mechanism of Li with transition metal oxides such as  $\text{Co}_3\text{O}_4$  differs from the classical mechanisms, which are based either on reversible insertion/deinsertion of lithium into host structures or on lithium alloying reactions.<sup>[3,15]</sup> Therefore, the electrochemical reaction mechanism of Li with porous  $\text{Co}_3\text{O}_4$  nanotubes in Li-battery can be described as follows:

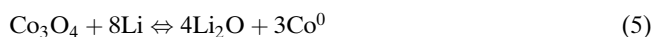
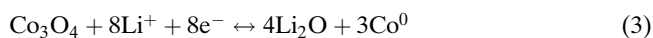
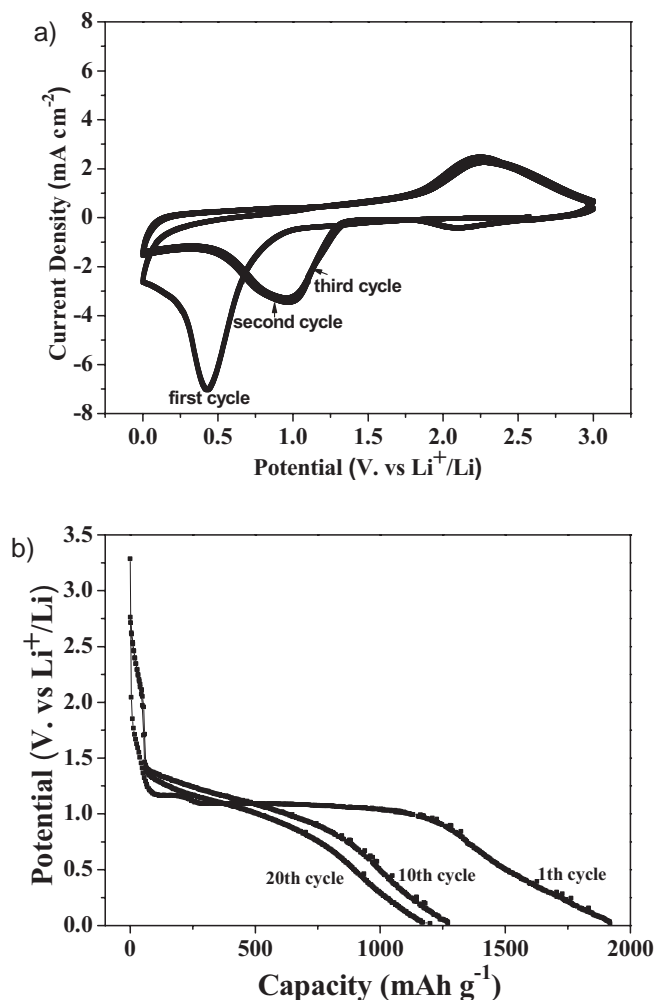


Figure 3a shows the first three cyclic voltammogram (CV) curves of the electrodes made from the porous  $\text{Co}_3\text{O}_4$  nanotubes at a scan rate of  $0.5 \text{ mVs}^{-1}$  and a temperature of  $20^\circ\text{C}$ .

The first discharge for the porous  $\text{Co}_3\text{O}_4$  nanotubes shows an irreversible reduction peak with a maximum at 0.4 V, which is different from the previous result due to the incomplete decomposition of  $\text{Co}_3\text{O}_4$ .<sup>[6]</sup> Compared to the first cycle, the discharge of the second and third cycles shows two peaks during cathodic polarization process attributed to two complete multistep redox reactions. While, in the anodic polarization process, one peak is recorded at about 2.2 V corresponding to oxidation of  $\text{Co}^0$  to  $\text{Co}^{3+}$ . Figure 3b shows the 1st, 10th, and 20th discharge curves of the electrodes made from the porous  $\text{Co}_3\text{O}_4$  nanotubes at a current density of  $50 \text{ mA g}^{-1}$  and a temperature of  $20^\circ\text{C}$ . In the first discharge curve, it can be seen that there are two sloping potential ranges for the lithium reaction during the first potential discharge, which is similar to the previous report.<sup>[6]</sup> During the 10th and 20th cycles, only one discharge slope is observed in the range (0.7–1.3V), with a decrease of the discharge capacity. The discharge capacities of the electrode in the 1st, 10th, and 20th cycles are 1918, 1269, and 1131  $\text{mAh g}^{-1}$ , respectively.

Figure 4 shows the discharge capacity versus cycle number for the electrodes made from the porous  $\text{Co}_3\text{O}_4$  nanotubes. Except the first cycle (about 1918  $\text{mAh g}^{-1}$ ), the capacity of other nineteen cycles is almost maintained constant at about 1200  $\text{mAh g}^{-1}$ , which shows the high capacity and good cycle life. To our best knowledge, the performance of the  $\text{Co}_3\text{O}_4$  based anode materials for lithium batteries presented here is the best up to now.<sup>[4a,6]</sup> The porous nanotube structures with the diameter of 30 nm consisting of the small nanoparticles



**Figure 3.** The first three CV curves of the porous  $\text{Co}_3\text{O}_4$  nanotube based anode materials at a scan rate of  $0.5 \text{ mVs}^{-1}$  and a temperature of  $20^\circ\text{C}$  (a); The 1st, 10th and 20th discharge curves of the porous  $\text{Co}_3\text{O}_4$  nanotube based anode materials at a current density of  $50 \text{ mA g}^{-1}$  and a temperature of  $20^\circ\text{C}$  (b).

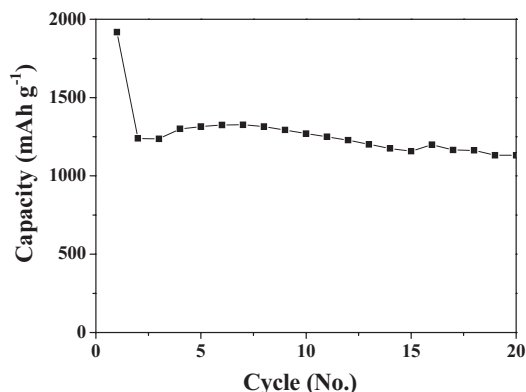


**Figure 4.** Discharge capacity versus cycle number for the porous  $\text{Co}_3\text{O}_4$  nanotube based anode materials at a current density of  $50 \text{ mA g}^{-1}$  and a temperature of  $20^\circ\text{C}$ .

with the size of about 5–10 nm are responsible for the improved performance. However, the initial coulombic efficiency for the porous  $\text{Co}_3\text{O}_4$  nanotubes is only about 70 %, which is similar to the previous reports.<sup>[15–17]</sup> It was considered that the formation of the solid electrolyte interface (SEI) film and some undecomposed  $\text{Li}_2\text{O}$  phase were responsible for the low initial coulombic efficiency.<sup>[16,17]</sup> In this paper, TEM image (Figs. S1a, S1b) and XRD pattern (Fig. S1c) of the porous  $\text{Co}_3\text{O}_4$  nanotube electrode taken from the first cycle indicate that the morphology and structure have been basically maintained after the first charge and discharge processes, which correspond to the previous reports.<sup>[7,16,17]</sup> Moreover, the Fourier transform infrared (FTIR) spectroscopy, as shown in Figure S1d, confirms the existence of  $\text{Li}_2\text{CO}_3$  and  $\text{ROCO}_2\text{Li}$ , which are the main components of SEI film. Therefore, it is believed that the formation of the SEI film may be the main reason for the low initial coulombic efficiency of the porous  $\text{Co}_3\text{O}_4$  nanotube electrode.

In summary, we have developed a novel and simple method to synthesizing the porous  $\text{Co}_3\text{O}_4$  nanotubes with the diameter of about 30 nm consisting of the small nanoparticles with the size of about 5–10 nm by the sonication in the hexane solution of  $\text{Co}_4(\text{CO})_{12}$  using CNTs as templates at room temperature and the subsequent calcination. The approach presented here can overcome the disadvantages of the AAO assisted method for the synthesis of the porous nanotubes, make it more suitable for Li-battery application. Moreover, the porous  $\text{Co}_3\text{O}_4$  nanotubes exhibit the superior Li-battery performance with good cycle life and high capacity ( $1200 \text{ mAh g}^{-1}$ ) due to the hollow structure and small size.

## Experimental

The carbon nanotubes (CNTs) with the diameter of about 30–50 nm were purchased from Times-nano Nanotech Co. Ltd. without further purification.  $\text{Co}_4(\text{CO})_{12}$  were purchased from Alfa Aesar China (Tianjin) Co. Ltd. The experimental details were as follows: Firstly, the CNTs were dispersed in hexane by the sonication for 1 h. Secondly, appropriate quantity of  $\text{Co}_4(\text{CO})_{12}$  were directly added into the above-mention solution and sonicated for 0.5 h. After the reaction completed, the resulted products were centrifugalized, washed with deionized water and ethanol to remove the ions possibly remaining in the final product, and dried at  $60^\circ\text{C}$  in air. Finally, the black powder was calcinated at  $500^\circ\text{C}$  in oxygen for 3 h.

The product was characterized by X-ray powder diffraction (XRD) using a Rigaku D/max-ga x-ray diffractometer with graphite monochromatized  $\text{CuK}\alpha$  radiation ( $\lambda = 1.54178 \text{ \AA}$ ). The images and structures of the sample were obtained by field emission scanning electron microscopy (FESEM, FEI SIRION), transmission electron microscopy (TEM, JEM 200 CX 160 kV) and high-resolution transmission electron microscope (HRTEM, JEOL JEM-2010F).

Electrochemical measurements were carried out using two-electrode cells with lithium metal as the counter and reference electrodes. The working electrodes were composed of the active material ( $\text{Co}_3\text{O}_4$  nanotubes), conductive material (acetylene black, ATB), and binder (polytetrafluoroethylene, PTFE) in a weight ratio of  $\text{Co}_3\text{O}_4/\text{ATB}/\text{PTFE} = 14:3:3$ . The electrode was dried at  $80^\circ\text{C}$  for 1 h and cut into a disk ( $1.0 \text{ cm}^2$ ). The electrolyte solution was 1M  $\text{LiPF}_6$  dissolved in a mixture of ethylene carbonate (EC), propylene carbonate (PC), and

diethyl carbonate (DEC) with the volume ratio of EC/PC/DEC = 3:1:1. The cell assembly was performed in a glove-box filled with pure argon (99.999 %) in the presence of an oxygen scavenger and a sodium drying agent. The electrode capacity was measured by a galvanostatic discharge-charge method at a current density of 50 mA g<sup>-1</sup> and 20 °C. Charge-discharge cycles were tested with a current density of 50 mA g<sup>-1</sup> in the potential range of 0.01–3.6V.

Received: November 6, 2006

Revised: August 2, 2007

- [1] a) Y. Idota, T. Kubota, A. Matsufuji, Y. Maekawa, T. Miyasaka, *Science* **1997**, 276, 1395. b) M. Winter, J. O. Besenhard, M. E. Spahr, P. Novak, *Adv. Mater.* **1998**, 10, 725. c) A. S. Arico, P. Bruce, B. Scrosati, J. M. Tarascon, W. V. Schalkwijk, *Nat. Mater.* **2005**, 4, 366.
- [2] J. M. Tarascon, M. Armand, *Nature* **2001**, 414, 359.
- [3] a) P. Poizot, S. Laruelle, S. Grugeon, L. Dupont, J. M. Tarascon, *Nature* **2000**, 407, 496. b) D. Larcher, D. Bonnin, R. Cortes, I. Rivals, L. Personaz, J. M. Tarascon, *J. Electrochem. Soc.* **2003**, 150, A1643.
- [4] a) K. T. Nam, D. W. Kim, P. J. Yoo, C. Y. Chiang, N. Meethong, P. T. Hammond, Y. M. Chiang, A. M. Belcher, *Science* **2006**, 312, 885. b) Y. M. Kang, M. S. Song, J. H. Kim, H. S. Kim, M. S. Park, J. Y. Lee, H. K. Liu, S. X. Dou, *Electrochim. Acta* **2005**, 50, 3667. c) X. P. Gao, J. L. Bao, G. L. Pan, H. Y. Zhu, P. X. Huang, F. Wu, D. Y. Song, *J. Phys. Chem. B* **2004**, 108, 5547. d) Y. Wang, H. C. Zeng, J. Y. Lee, *Adv. Mater.* **2006**, 18, 645. e) S. J. Han, B. C. Jang, T. Kim, S. M. Oh, T. Hyeon, *Adv. Funct. Mater.* **2005**, 15, 1845. f) Y. Yu, C. H. Chen, J. L. Shui, S. Xie, *Angew. Chem. Int. Ed.* **2005**, 44, 2. g) I. Moriguchi, R. Hidaka, H. Yamada, T. Kudo, H. Murakami, N. Nakashima, *Adv. Mater.* **2006**, 18, 69.
- [5] a) T. He, D. R. Chen, X. L. Jiao, *Chem. Mater.* **2004**, 16, 737. b) B. B. Lakshmi, C. J. Patrissi, C. R. Martin, *Chem. Mater.* **1997**, 9, 2544. c) Y. Liu, G. Wang, C. Xu, W. Wang, *Chem. Commun.* **2002**, 1486.
- [6] W. Y. Li, L. N. Xu, J. Chen, *Adv. Funct. Mater.* **2005**, 15, 851.
- [7] a) J. Chen, L. N. Xu, W. Y. Li, X. L. Gou, *Adv. Mater.* **2005**, 17, 582. b) H. Tan, E. Y. Ye, W. Y. Fan, *Adv. Mater.* **2006**, 18, 619. c) X. X. Li, F. Y. Cheng, B. Guo, J. Chen, *J. Phys. Chem. B* **2005**, 109, 14017. d) W. Y. Li, S. Y. Zhang, J. Chen, *J. Phys. Chem. B* **2005**, 109, 14025.
- [8] Z. Y. Sun, H. Q. Yuan, Z. M. Liu, B. X. Han, X. R. Zhang, *Adv. Mater.* **2005**, 17, 2993.
- [9] B. C. Satishkumar, A. Govindaraj, E. M. Vogel, L. Basumalick, C. N. Rao, *J. Mater. Res.* **1997**, 12, 604.
- [10] W. Han, A. Zettl, *Nano Lett.* **2003**, 3, 681.
- [11] a) Z. Sun, H. Yuan, B. Han, X. Zhang, *Adv. Mater.* **2005**, 17, 2993. b) S. Bae, H. Seo, H. Choi, J. Park, *J. Phys. Chem. B* **2004**, 108, 12318. c) J. Ye, H. Cui, X. Liu, T. Lim, W. Zhang, F. Sheu, *Small* **2005**, 1, 560.
- [12] N. Du, H. Zhang, B. D. Chen, X. Y. Ma, Z. H. Liu, J. B. Wu, D. R. Yang, *Adv. Mater.* **2007**, 19, 1641.
- [13] a) V. F. Puentes, K. M. Krishnan, A. P. Alivisatos, *Science* **2001**, 291, 2115. b) A. C. S. Samia, K. Hyzer, J. A. Schlueter, C. J. Qin, J. S. Jiang, S. D. Bader, X. M. Lin, *J. Am. Chem. Soc.* **2005**, 127, 4126.
- [14] Y. S. Min, E. J. Bae, K. S. Jeong, Y. J. Cho, J. H. Lee, W. B. Choi, G. S. Park, *Adv. Mater.* **2003**, 15, 1019.
- [15] P. Poizot, S. Larunelle, S. Grugeon, J. M. Tarascon, *J. Electrochem. Soc.* **2002**, 149, A1212.
- [16] Y. M. Kang, K. T. Kim, K. Y. Lee, S. J. Lee, J. H. Jung, J. Y. Lee, *J. Electrochem. Soc.* **2003**, 150, A1538.
- [17] Y. M. Kang, M. S. Song, J. H. Kim, H. S. Kim, M. S. Park, J. Y. Lee, H. K. Liu, S. X. Dou, *Electrochim. Acta* **2005**, 50, 3667.